

Semantic-guided Automatic Natural Image Matting with Light-weight Non-local Attention

Yuhongze Zhou^{1,2}, Liguang Zhou^{1,2}, Tin Lun Lam^{*1,2}, and Yangsheng Xu^{1,2}

¹The Chinese University of Hong Kong, Shenzhen

²Shenzhen Institute of Artificial Intelligence and Robotics for Society

3160104220@zju.edu.cn, {liguangzhou@link., tllam@, ysxu@}cuhk.edu.cn

Abstract

Natural image matting aims to precisely separate foreground objects from background using alpha matte. Fully automatic natural image matting without external annotation is quite challenging. Well-performed matting methods usually require accurate labor-intensive handcrafted trimap as extra input, while the performance of automatic trimap generation method of dilating foreground segmentation fluctuates with segmentation quality. Therefore, we argue that how to handle trade-off of additional information input is a major issue in automatic matting. This paper presents a universal semantic-guided automatic natural image matting pipeline with light-weight non-local attention without trimap and background image as input. Specifically, guided by semantic information of coarse foreground segmentation, Trimap Generation Network estimates accurate trimap. With estimated trimap and RGB image as input, our light-weight Non-local Matting Network with Refinement produces final alpha matte, whose trimap-guided global aggregation attention block is equipped with stride downsampling convolution, reducing computation complexity and promoting performance. Experimental results show that our matting algorithm has competitive performance with current state-of-the-art methods in both trimap-free and trimap-needed aspects.

1. Introduction

Image matting is a popular image editing task which attempts to extract perfect foreground object mask, i.e. alpha matte, from background. Matting problem can be formulated in a general mathematical manner. An image I can be defined as a combination weight, which is represented by

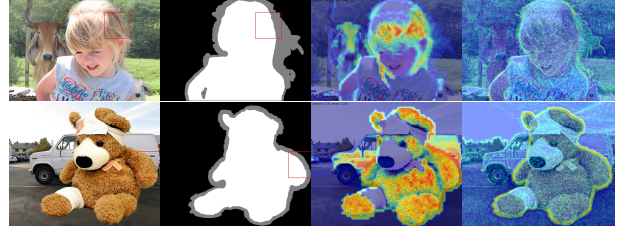


Figure 1: The visualization of our attention block. From left to right, image, trimap, global attention weight map of given query patch marked by red box, and reconstructed alpha feature of attention block.

alpha matte α , of foreground F and background B image as follows:

$$I = \alpha F + (1 - \alpha)B, \quad (1)$$

where the three-channel RGB color I is known, but the RGB color F , B and alpha matte α are unknown. That is to say, matting attempts to solve 7 unknown variables with only 3 known ones provided. Therefore, most compelling matting methods usually require a handcrafted trimap for region constrain to reduce complexity and assist matte estimation, which makes fully-automatic natural image matting such an appealing and worthy task to explore.

Let us recap recent learning-based image matting approaches and their pros and cons. Learning-based image matting can be divided into three primary categories, i.e. background-required [43, 47], only-image [44, 66] input, and trimap-needed [14, 60, 39, 37, 54, 32].

Recently, novel background matting [47, 34] is proposed, but it cannot resist the interference of shadows or complex light condition. For algorithms requiring nothing but to-be-matted image [44, 66], results on generic objects are far from practical expectations. Although human mat-

*Corresponding Author

ting, one branch of trimap-free matting, has achieved impressive performance [49, 10, 36, 27], human is regarded as such a specific domain and salient object that it is relatively easy for network to capture foreground/background discrepancy. So does animal image matting [31].

For trimap-needed matting, its accuracy is paramount, which gives the credit to auxiliary trimap that makes relation modeling between known and unknown areas possible. The trimap provides deterministic foreground, unknown, and background regions of image, which narrows down matte estimation to unknown region and reset pixel values of known region. Hence, trimap quality is one significant factor that can affect matting performance. Besides, as accurate trimap-needed matting is, the manual creation of trimap is painstaking, which causes its less powerful application potential. One possible workaround in practice is a general automatic trimap generation method, that is, target foreground items are roughly extracted by semantic segmentation and then processed by image dilation/erosion. Regarding this way, the quality of semantic segmentation has a dominant influence on corresponding trimap, similar to what trimap is to matte.

From the above-mentioned problems, it is obvious that **trimap-needed matting (mentioned trimap generation method) has a trimap (foreground segmentation) quandary**. Although previous methods attempt to solve these puzzles, they mainly focus on single-category matting by exploring refining trimap to boost matting results [49, 8], employing implicit trimap to assist human/animal matting without trimap input [10, 66, 31], and coupling coarse annotated data with fined one to promote human matting [36], which **are hard to generalize to comprehensive data and usually require salient single-category object**.

Considering forementioned issues, we argue that how to find a balance between extra knowledge and matte accuracy is a critical cornerstone for automating natural image matting. Therefore, we disentangle automatic matting into trimap and alpha estimation subtasks as workaround. Different from all past attempts, we aim to generalize trimap-free matting more properly to comprehensive data. We propose a semantic-guided trimap-free matting approach, which consists of Trimap Generation Network and light-weight Non-local Matting Network with Refinement Module. Coarse foreground segmentation provides additional semantic information and can help network capture rough location and shape of target object, which can be easily obtained by salient/segmentation models. Therefore, Trimap Generation Network employs coarse foreground segmentation as guidance to estimate a proper trimap. This estimated trimap serves as guidance for matting network and also buffer for negative trimap quality chain reaction. Our proposed light-weight non-local attention block utilizes stride downsampling convolution to reduce similarity computa-

tion cost and rearranges alpha feature by propagating the global pixel-to-pixel relationship of image feature on an explicit fashion. Refinement module with fusion techniques bridges two main components together to produce high-quality alpha matte without trimap and background as input. Trimap Generation Network is validated to be segmentation fault-tolerance and qualified for matting task. Extensive experiments show that our matting pipeline has comparable performance with other state-of-the-art methods on the Composition-1k testset, alphamattng.com benchmark, and Distinctions-646 testset. To demonstrate real-world application capability of our proposed pipeline, we conduct real data adaption by finetuning our framework on real imagery data guided by pretrained teacher matting network and a discriminator that judges the composite realism.

The main contribution of this work is threefold. First, we propose a novel two-stage trimap-free natural image matting approach boosted by coarse foreground segmentation and our light-weight non-local attention, which refreshes the state-of-the-art matting record in trimap-needed and trimap-free respects. Our proposed method finds a trade-off between additional information and performance. **We believe that this matting architecture should be more rational trimap-free matting framework, which has comprehensive integration ability with other semantic segmentation/salient object detection/matting approaches to better solve automatic natural image matting.** Second, we propose Trimap Generation Network to predict the possibility of each pixel belonging to foreground, background, and unknown areas for matting purpose, which can better capture semantic information and still provide accurate trimap for defective segmentation input. Third, our light-weight attention layer not only reduces computational complexity but also maintains effective performance.

2. Related Works

Natural Image Matting: Traditional image matting can be roughly classified into two categories, sampling-based [15, 56, 57, 18, 22, 48, 2] and propagation-based [11, 19, 28, 29, 30, 52] approaches, which usually require trimap as additional input. Recently, matting techniques using deep learning have shown increasingly prominent performance, which can be categorized into three domains, i.e., trimap-needed [14, 60, 39, 37, 54, 32, 63], background-required [43, 47, 34] and only-image [1, 66, 44] input. After Cho *et al.* [14] introduce deep neural networks into image matting task, Xu *et al.* [60] propose a deep neural network matting solution with a comprehensive matting database which has promoted research progress significantly. Lutz *et al.* [39] explore matting task with a generative adversarial framework. Then, appealing matting results are achieved by Lu *et al.* [37] and Tang *et al.* [54]. Subsequently, a state-of-the-art matting method with guided contextual at-

tention is proposed, which not only simulates information flow of affinity-based methods but also models matting in a view of image inpainting [32]. Given an image, its corresponding background, and soft segmentation, background matting [47] is adapted to real human data and obtain appealing estimation but is not robust to images with shadow or under complex light conditions. Since trimap-needed matting algorithm usually requires high-quality handmade trimap, whose producing process is time-consuming, a few works are attempting to take only image as input and produce matte [66, 44]. However, these trimap-free methods are not capable of producing comparable quality matte.

Attention Mechanism: Attention mechanism has been widely utilized in deep learning tasks, e.g. machine translation [6, 38, 7, 55, 53], image classification [41, 26], image generation [20, 16, 42], object detection [5], image synthesis [65], video classification [59], and semantic segmentation [17, 25]. The self-attention block is introduced to transform and contributes to each position of output by referring to every position of input [55]. Similarly, Wang *et al.* [59] propose non-local attention to acquire long-range contextual information and promote video classification tasks. Instead of capturing long-term dependencies in sequences, recently, attention has shown its superiority in image matting [32, 44, 63], by making network capture structural pixel-to-pixel dependencies of image that can deepen semantic understanding of matting network. Li *et al.* [32] simulate non-local attention by convolution and deconvolution to enhance alpha matte estimation. Qiao *et al.* [44] use channel/spatial-wise attention to filter out noise from hierarchical appearance cues and boost alpha mattes. Yu *et al.* [63] introduce three non-local attentions to propagate each trimap region of context patches to corresponding region of query patches and achieve high-resolution image matting with cross-patch modeling. However, our approach leverages only one attention layer and has better matting performance.

Trimap Generation: Automatic trimap generation, which is popular in traditional matting [58, 24, 51, 21, 12], usually contains two steps: binary segmentation for foreground/background separation and image erosion/dilation. These methods mainly differentiate in how to obtain segmentation. For example, Wang *et al.* [58] leverage depth information to compute segmentation; Gupta *et al.* [21] combine salient object detection with superpixel analysis for segmentation; Hsieh *et al.* [24] use graph cuts for foreground extraction; Chen *et al.* [12] require user to indicate foreground/background by a few clicks and apply one-shot learning for binary mask prediction. Besides, Al-Kabbany *et al.* [3] first introduce the Gestalt laws of grouping to matting that assists more robust trimap generation. Cho *et al.* [13] integrate depth map with color distribution based processing for foreground/background separa-

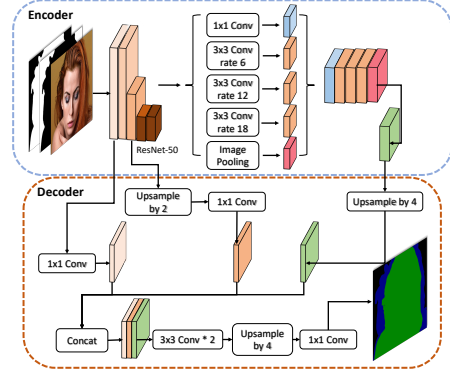


Figure 2: Trimap Generation Network (Net-T)

tion by graph cut followed by unknown region detection for trimap generation. Recently, neural networks have been utilized to generate implicit trimap for human matting automation [49, 10].

3. Approach

We decompose our trimap-free matting approach into two parts. The first one, **Trimap Generation Network (Net-T)**, with rough object segmentation [62, 9] as an indicator, understands target object shape and its relation with surroundings to perform accurate pixel-wise classification among foreground/background/unknown regions. The second one, **light-weight Non-local Matting with Refinement (Net-M)**, utilizes an RGB image and the output of Net-T to estimate an alpha matte. The overview of our proposed matting framework is illustrated in Fig. 4.

3.1. Trimap Generation Network (Net-T)

Trimap estimation can be seen as a 3-class semantic segmentation. The output of Net-T is a 3-channel feature map indicating the possibility that each pixel is assigned to each of the 3 classes. The input of Net-T is a cropped RGB image and a 2-channel one-hot soft foreground segmentation which are concatenated as a 5-channel input. We modified Deeplabv3 [9] as the encoder by adjusting the input channel size and taking the first two channel weights of *conv_1* of the pretrained ResNet-50 as the weight of 2-channel segmentation. Instead of using its original decoder, we propose our own decoder to reconstruct semantic information, as illustrated in Fig. 2. The dropout layer by a factor of 0.5 is first applied to the encoder feature, followed by a four-time bilinearly upsampling. Then, it is concatenated with low and middle-level features of the backbone for final classification. The swapped order of upsampling and final convolution makes classification more fine-grained. Except for the high-level encoder feature, low and middle-level features enrich the decoding process and make the network pay

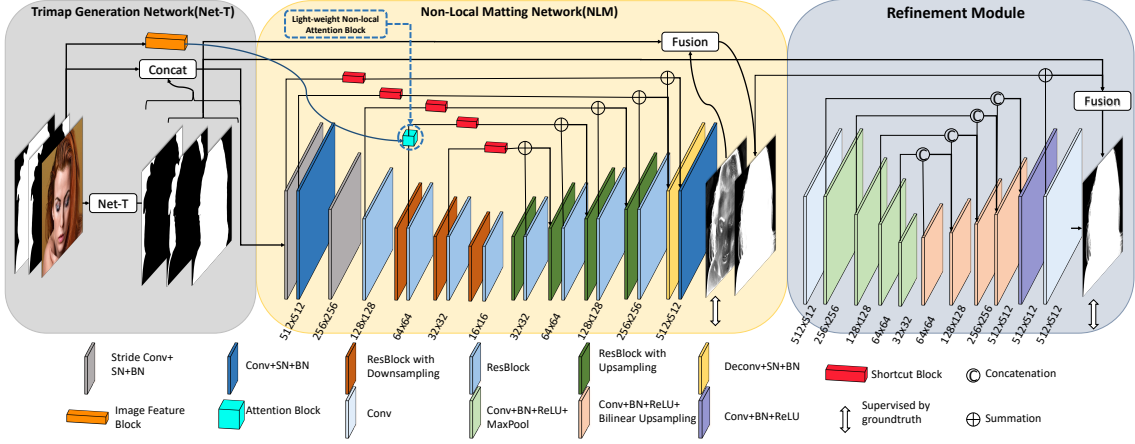


Figure 4: The Overview of our Matting Pipeline. Non-local Matting Network with Refinement Module is Net-M. Net-T and Net-M collaborative testing is Joint Inference. (SN is Spectral Normalization, while BN is Batch Normalization.)

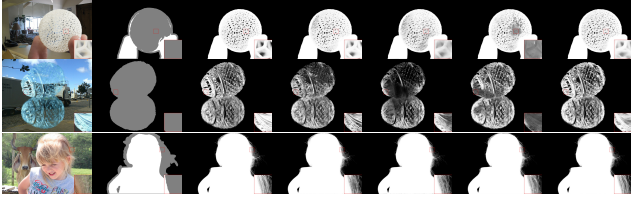


Figure 5: Comparison of visual results of the Composition-1k test dataset of different methods. From left to right, the original image, dataset-provided trimap, GT alpha matte, IM [37], CAM-3¹ [23], GCA [32], Net-M

samples to automatically guide the model to focus more on hard alpha region. The hard mining loss is defined as $L_{hard} = \frac{1}{|\mathcal{H}\mathcal{M}|} \sum_{i \in \mathcal{H}\mathcal{M}} |\hat{\alpha}_i - \alpha_i|$, where $\mathcal{H}\mathcal{M}$ means the region that contains hard samples, $\hat{\alpha}_i, \alpha_i$ indicate the predicted and ground-truth alpha at position i and $p = 50$ in our experiments.

4. Experiment Settings and Results

4.1. Experiment Settings

We train Net-T and Net-M separately and then test the whole net jointly with fusion techniques [10] (Joint Inference).

Net-T: For random soft segmentation input generation, random trimap is the first step, which is produced by random erosion on both foreground and background of alpha ranging from 1 to 29 pixels [32]. The unknown and foreground areas of random trimap is considered as foreground

¹CAM with Matting Encoder(ME)+Context Encoder(CE)+Laplacian loss(lap)+feature loss(fea)+color loss(color)+Data Augmentation(DA)

| AIM | | | | | |
|-----------|--------------------|---------------|------------------|-------------|---------------|
| Methods | Evaluation metrics | | | | |
| | Accuracy | mean Bg IoU | mean Unknown IoU | mean Fg IoU | mIoU |
| Net-T | 0.9641 | 0.9353 | 0.8278 | 0.7064 | 0.8232 |
| Deeplabv3 | 0.9583 | 0.9159 | 0.8025 | 0.7066 | 0.8083 |
| Deeplabv2 | 0.9358 | 0.8981 | 0.7625 | 0.6309 | 0.7638 |

| Distinctions-646 | | | | | |
|------------------|--------------------|---------------|------------------|---------------|---------------|
| Datasets | Evaluation metrics | | | | |
| | Accuracy | mean Bg IoU | mean Unknown IoU | mean Fg IoU | mIoU |
| Net-T | 0.9574 | 0.9654 | 0.8083 | 0.6672 | 0.8136 |
| Deeplabv3 | 0.9566 | 0.9511 | 0.7965 | 0.6552 | 0.8009 |
| Deeplabv2 | 0.9258 | 0.9440 | 0.7297 | 0.5382 | 0.7373 |

Table 1: The quantitative comparison of Net-T with adapted Deeplabv3 and Deeplabv2 on Adobe Image Benchmark testset and Distinctions-646 testset.

of random *initial segmentation*. Then, random soft segmentation is generated by eroding and dilating random *initial segmentation* sequentially with random number of pixels ranging from 1 to 59 and followed by a random Gaussian Blur [47]. To obtain *synthesized ground-truth trimap* for supervision, we apply 15-pixel erosion on the both foreground and background of alpha. Image patches are randomly cropped from input images and then resized to 512×512 . We train Net-T for 129,300 iterations with a batch size of 10. The learning rate is initialized to 0.001 and adjusted every iteration.

Net-M: We follow the same data processing and augmentation procedure as GCA-Matting [32]. Net-M is trained for 400,000 iterations with a batch size of 20 with $L_{coarse-\alpha} + L_{refined-\alpha}$ as the regression loss and unknown region of trimap as \mathcal{M} . The adam optimizer with $\beta_1 = 0.5$ and $\beta_2 = 0.999$ is adopted with initialized learning rate, 4×10^{-4} , plus warmup and cosine decay techniques.

Joint Inference (JI): Joint Inference is Net-T and Net-

M collaborative testing by adopting Net-T-predicted trimap as one input of Net-M. Since categories of foreground objects of synthesized matting datasets may not match popular segmentation datasets, and background objects may have the same category as foreground and can also be salient, salient/segmentation models may not be suitable for coarse segmentation generation. Therefore, JI setting here is for synthesized datasets (For real data, we provide transfer approach in Real World Human Data part of section 4.2.2.). The soft segmentation input for testing is generated by erosion on *initial segmentation* from *synthesized ground-truth trimap* with 20 pixels and followed by a Gaussian Blur. In Fig. 4, the raw alpha estimation of Net-M is far away from impressive except the unknown region. Hence, we propose two fusion methods to solve this. One is probability-based soft fusion, another is region-based hard fusion. For soft fusion, we use region probabilities estimated by Net-T to reconstruct final alpha α_r from predicted alpha α_p [10] as $\alpha_r = (1 - U_p) \frac{F_p}{F_p + B_p} + U_p \alpha_p$, $U_p = 1 - (F_p + B_p)$ and $\alpha_r = F_p + U_p \alpha_p$, where U_p , F_p , and B_p are probabilities of each pixel belonging to unknown, foreground, and background regions severally. For hard fusion, we reset trimap-predicted foreground and background to 255 and 0 on predicted alpha respectively.

4.2. Experiment Results

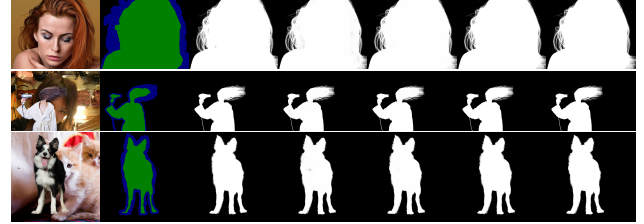
4.2.1 Evaluation on trimap

We evaluate Net-T and other popular adapted semantic segmentation methods, e.g. Deeplabv3 and Deeplabv2, on Composition-1k and Distinctions-646 testset, by using pixel classification accuracy and mean IoU metrics of foreground, unknown, background, and three-region-involved. Results in Table 1 shows that trimap segmentation accuracy and mIoU metrics of Net-T are superior to other methods. Considering quantitative results in Table 1 and visual examples presented in Fig. 6, our trimap estimation is competent to mentor Net-M.

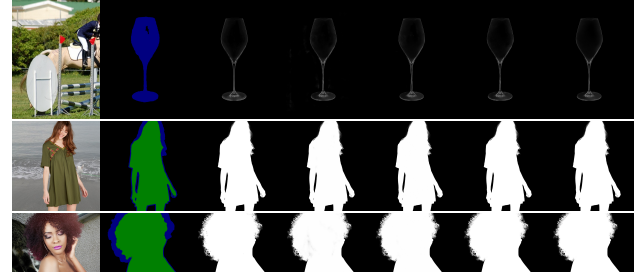
4.2.2 Evaluation on alpha matte

In this section, we follow common evaluation metrics, i.e. Sum of Absolute Differences (SAD), Mean Squared Error (MSE), Gradient error (Grad), and Connectivity error (Conn) to evaluate our approaches on popular matting datasets, including Composition-1k testset, alphamating.com benchmark, and Distinctions-646 benchmark. To validate unlabeled real-world adaption ability of our two-stage approach, we choose human as a typical illustration case and conduct a user study for evaluation.

Adobe Image Matting Benchmark (AIM): We follow composition rules Xu *et al.* proposed [60] to synthesize 43,100 training images and 1,000 testing images and compare our approach and its ablation study results with



(a) Composition-1k testset



(b) Distinctions-646 benchmark

Figure 6: Ablation comparison of visual results of Joint Inference with Fusion on different benchmarks. From left to right, image, trimap predicted by Net-T, GT, JIS-c, JIS, JIH-c, and JIH.



Figure 7: Comparison of visual results of real data between CAM-1 and our JI-Real. From left to right, image, CAM-1 and JI-Real.

other state-of-the-art matting methods in Table 3. From Table 3, in the perfect trimap provided situation, Net-M exhibits dominating performance on all four metrics compared with other state-of-the-art methods. Also, from the ablation study, the complete Net-M system possesses three out of four superior metrics except for Gradient error, compared to Net-M without hard mining loss (Net-M-nh) and Net-M without refinement (NLM), which demonstrates the effectiveness of each part of our system. In the trimap-free case, the comparison between our JI and approaches marked by [†] reveals much more improvement of JI on MSE, Grad, and Conn metrics. In Fig. 5 and 6 (a), we represent the qualitative comparison between our approaches and other state-of-the-art methods in both settings. Given additional

| SAD | Average Rank | | | | Troll | | | Doll | | | Donkey | | | Elephant | | | Plant | | | Pineapple | | | Plastic bag | | | Net | | |
|---|--------------|------------|------------|------|-------|------|------|------|-----|-----|--------|-----|-----|----------|-----|-----|-------|-----|-----|-----------|-----|-----|-------------|------|------|------|------|------|
| | Overall | S | L | U | S | L | U | S | L | U | S | L | U | S | L | U | S | L | U | S | L | U | S | L | U | S | L | U |
| Non-local Matting with Refinement(Ours) | 6.5 | 5.8 | 5.9 | 8 | 7 | 8.1 | 8.1 | 4.2 | 4.4 | 5.4 | 2.6 | 2.6 | 2.3 | 1 | 1 | 1.2 | 4.9 | 5.8 | 7.6 | 2.1 | 2.2 | 3.2 | 19.7 | 22.5 | 19.9 | 20.1 | 20.9 | 24.7 |
| HDMatt[63] | 7.3 | 9.3 | 6 | 6.8 | 9.5 | 10 | 10.7 | 4.7 | 4.8 | 5.8 | 2.9 | 3 | 2.6 | 1.1 | 1.2 | 1.3 | 5.2 | 5.9 | 6.7 | 2.4 | 2.6 | 3.1 | 17.3 | 17.3 | 17 | 21.5 | 22.4 | 23.2 |
| AdaMatting[8] | 9.1 | 7.9 | 8.1 | 11.4 | 10.2 | 11.1 | 10.8 | 4.9 | 5.4 | 6.6 | 3.6 | 3.4 | 3.4 | 0.9 | 0.9 | 1.8 | 4.7 | 6.8 | 9.3 | 2.2 | 2.6 | 3.3 | 19.2 | 19.8 | 18.7 | 17.8 | 19.1 | 18.6 |
| SampleNet Matting[54] | 9.5 | 7.6 | 9.1 | 11.9 | 9.1 | 9.7 | 9.8 | 4.3 | 4.8 | 5.1 | 3.4 | 3.7 | 3.2 | 0.9 | 1.1 | 2 | 5.1 | 6.8 | 9.7 | 2.5 | 4 | 3.7 | 18.6 | 19.3 | 19.1 | 20 | 21.6 | 23.2 |
| GCA Matting[32] | 10.7 | 11.8 | 7.9 | 12.5 | 8.8 | 9.5 | 11.1 | 4.9 | 4.8 | 5.8 | 3.4 | 3.7 | 3.2 | 1.1 | 1.2 | 1.3 | 5.7 | 6.9 | 7.6 | 2.8 | 3.1 | 4.5 | 18.3 | 19.2 | 18.5 | 20.8 | 21.7 | 24.7 |

Table 2: Top-5 SAD results on alphamattng.com benchmark, where S, L, U represent the trimap type of small, large and user, and bold numbers show that our Non-local Matting with Refinement achieves the best SAD performance at the time of submission.

| Trimap-needed Evaluation | | | | |
|--|--------------------|----------------|--------------|--------------|
| Methods | Evaluation metrics | | | |
| | SAD | MSE | Grad | Conn |
| AlphaGAN[39] | 52.4 | 0.03 | 38 | 53 |
| Deep Image Matting[60] | 50.4 | 0.014 | 30.0 | 50.8 |
| IndexNet Matting(IM)[37] | 45.8 | 0.013 | 25.9 | 43.7 |
| AdaMatting[8] | 41.7 | 0.01 | 16.8 | - |
| Learning Based Sampling[54] | 40.35 | 0.0099 | - | - |
| Context-Aware Matting(CAM)[23] | 35.8 | 0.0082 | 17.3 | 33.2 |
| GCA-Matting(GCA)[32] | 35.28 | 0.0091 | 16.92 | 32.53 |
| HDMatt[63] | 33.5 | 0.0073 | 14.5 | 29.9 |
| Net-M | 29.43 | 0.00602 | 12.27 | 25.80 |
| Net-M w/o L_{hard} (Net-M-nh) | 30.75 | 0.00627 | 13.12 | 27.31 |
| Non-local Matting(NLM) | 29.77 | 0.00605 | 11.96 | 26.10 |
| Trimap-free Evaluation | | | | |
| Methods | Evaluation metrics | | | |
| | SAD | MSE | Grad | Conn |
| Late Fusion [†] [66] | 58.34 | 0.011 | 41.63 | 59.74 |
| HAttMatting [†] [44] | 44.01 | 0.007 | 29.26 | 46.41 |
| JIS [†] | 43.91 | 0.00542 | 18.64 | 39.82 |
| JIS w/o refinement(JIS-c) [†] | 47.43 | 0.00553 | 18.61 | 41.43 |
| JIH [†] | 41.85 | 0.00551 | 18.34 | 39.42 |
| JIH w/o refinement(JIH-c) [†] | 42.39 | 0.00556 | 18.59 | 39.87 |

Table 3: The quantitative results on Composition-1k testset. (- indicates not given in the original paper. [†] means that all metrics are calculated on the whole image. JIS and JIH means JI with soft and hard fusion respectively. JIS, JIH, -, and [†] express forementioned meanings through the entire paper.)

| Methods | Evaluation metrics | | | |
|--------------------------------------|--------------------|----------------|--------------|--------------|
| | SAD | MSE | Grad | Conn |
| Deep Image Matting [†] [60] | 47.56 | 0.009 | 43.29 | 55.90 |
| HAttMatting [†] [44] | 48.98 | 0.009 | 41.57 | 49.93 |
| JIS [†] | 41.91 | 0.00795 | 38.38 | 39.46 |
| JIS-c [†] | 46.14 | 0.00789 | 36.74 | 40.13 |
| JIH [†] | 38.52 | 0.00796 | 38.23 | 38.28 |
| JIH-c [†] | 39.33 | 0.00808 | 38.48 | 38.76 |

Table 4: The quantitative results on Distinctions-646 testset.

carefully-prepared trimap, our approach is capable of obtaining more fine-grained details of transparent objects than others do. Considering a scenario where there is an image whose potential target foreground objects are non-salient or occluded with other equally conspicuous objects in varie-

gated backgrounds, common trimap-free matting [66, 44] that leverages a single RGB image as input is struggling for which object should be extracted. However, our JI strategy smartly decomposes automatic matting into two steps and circumvents this drawback.

AlphaMatting.com Benchmark: The submitted methods on this benchmark [45] are ranked by the averaged ranking over 24 alpha matte estimations according to different metrics. In Table 2, our Non-local Matting with Refinement achieves the best SAD result among the state-of-the-art methods on the alphamattng.com benchmark at the time of submission as well as satisfactory performance on the other three metrics at the same time².

Distinctions-646 Benchmark: Qiao *et al.* establish the Distinctions-646 dataset, consisting of 646 diversified foreground images [44] which is more miscellaneous than AIM. Following the same composition rule as AIM, we synthesize 59,600 images for training and 1,000 images for testing. The Table 4 shows the quantitative comparison between our approach and baseline. Our JI approach with either fusion technique exceeds HAttMatting and Deep Image Matting in SAD and Conn metrics by a solid margin. The Fig. 6 (b) indicates that, after refinement module and the secondary fusion, much deterioration part of coarse matte is removed, which mainly benefits from our semantic-guided network architecture design.

Real World Human Data: To demonstrate application capability of our approach, we adopt similar adversarial training for real data adaption as Sengupta *et al.* [47]. We capture 37 handheld videos, in which the subject is moving around and the camera is moved randomly, and combine them with 10 real-world videos from Background Matting [47] for training. We retrain AIM-pretrained matting pipeline (JI-Real) end-to-end using soft fusion on 22,144 real-world video frames. Net-T of JI-Real is supervised by pseudo trimap generated by segmentation [62] and erosion/dilation, while human-finetuned Net-M serves as a teacher for Net-M of JI-Real. End-to-end training and interaction between generator (JI-Real) and discriminator help JI-Real jump out of the local minimum of human-finetuned

²Please refer to supplementary materials for visual comparison and more quantitative results

| Composition-1k testset | | | | |
|------------------------|--------------------|-------------|------------------|--------|
| Methods | Evaluation metrics | | | |
| | Accuracy | mean Bg IoU | mean Unknown IoU | mIoU |
| Net-T-20 | 0.9641 | 0.9353 | 0.8278 | 0.7064 |
| Net-T-30 | 0.9634 | 0.9326 | 0.8257 | 0.7046 |
| Net-T-40 | 0.9616 | 0.9277 | 0.8174 | 0.7014 |
| Net-T-50 | 0.9590 | 0.9225 | 0.8058 | 0.6949 |

| Distinctions-646 testset | | | | |
|--------------------------|--------------------|-------------|------------------|--------|
| Methods | Evaluation metrics | | | |
| | Accuracy | mean Bg IoU | mean Unknown IoU | mIoU |
| Net-T-20 | 0.9574 | 0.9654 | 0.8083 | 0.6672 |
| Net-T-30 | 0.9566 | 0.9620 | 0.8022 | 0.6682 |
| Net-T-40 | 0.9557 | 0.9600 | 0.7960 | 0.6694 |
| Net-T-50 | 0.9531 | 0.9568 | 0.7834 | 0.6672 |

(a) Net-T

| Composition-1k testset | | | | |
|--------------------------|--------------------|---------|-------|-------|
| Methods | Evaluation metrics | | | |
| | SAD | MSE | Grad | Conn |
| Late Fusion [†] | 58.34 | 0.011 | 41.63 | 59.74 |
| HAttMatting [†] | 44.01 | 0.007 | 29.26 | 46.41 |
| JIS [†] -20 | 43.91 | 0.00542 | 18.64 | 39.82 |
| JIS [†] -30 | 44.24 | 0.00550 | 18.75 | 40.10 |
| JIS [†] -40 | 44.64 | 0.00564 | 18.92 | 40.43 |
| JIS [†] -50 | 45.55 | 0.00589 | 19.47 | 41.24 |
| JIH [†] -20 | 41.85 | 0.00551 | 18.34 | 39.42 |
| JIH [†] -30 | 42.08 | 0.00559 | 18.42 | 39.66 |
| JIH [†] -40 | 42.29 | 0.00571 | 18.53 | 39.87 |
| JIH [†] -50 | 43.00 | 0.00595 | 19.05 | 40.54 |

| Distinctions-646 testset | | | | |
|--------------------------------------|--------------------|---------|--------|--------|
| Methods | Evaluation metrics | | | |
| | SAD | MSE | Grad | Conn |
| Deep Image Matting [†] [60] | 47.56 | 0.009 | 43.29 | 55.90 |
| HAttMatting [†] [44] | 48.98 | 0.009 | 41.57 | 49.93 |
| JIS [†] -20 | 41.909 | 0.00795 | 38.379 | 39.459 |
| JIS [†] -30 | 41.96 | 0.00787 | 38.382 | 39.458 |
| JIS [†] -40 | 42.401 | 0.00793 | 39.522 | 39.791 |
| JIS [†] -50 | 43.917 | 0.00829 | 40.857 | 41.272 |
| JIH [†] -20 | 38.52 | 0.00796 | 38.23 | 38.28 |
| JIH [†] -30 | 38.39 | 0.00783 | 37.774 | 38.170 |
| JIH [†] -40 | 38.577 | 0.00787 | 38.661 | 38.374 |
| JIH [†] -50 | 39.880 | 0.00825 | 40.269 | 39.736 |

(b) JI

Table 5: Comparison of different segmentation inputs for Net-T and JI on different datasets. (<network>-X, like Net-T-X, JIS-X and JIH-X, means that segmentation is generated by erosion on *initial segmentation* from *synthesized ground-truth trimap* with X pixels and followed by a Gaussian Blur.)

| Methods | # parameters | GFLOPs |
|-------------------------|--------------|--------|
| Non-local Matting(Ours) | 25,984 | 0.1416 |
| GCA-Matting [32] | 49,792 | 3.5621 |

Table 6: Comparison of the number of parameters and GFLOPs of attention block between our Non-local Matting and GCA-Matting [32]

Net-M.³ For testing, we combine other 5 self-captured videos and 5 videos from Background Matting [47], and then the testset consists of 100 images that are formed by 10 uniformly-sampled frames from each test video. In the

³Please refer to supplementary materials for training details.

user study, we composite matte on black background and compare JI-Real with Context-Aware Matting [23] on 100 testing images. Each user was presented with one web page, showing 100 pairs of original image, composite of JI-Real and CAM-1⁴ with the random order of the last two. Participants are asked to rate the left composite relative to the right on three scales, i.e. better, similar and worse. We survey 10 users and our method achieves 65.8% better, 28.7% similar but only 5.5% worse than CAM-1, which implies the competitive performance of our trimap-free pipeline compared to modest trimap-needed matting on real-world human images with diverse backgrounds. Fig. 7 shows the visual comparison. This experiment validates that our approach can be trained to adapt to different domains of soft segmentation, therefore, we are confident about practical value of our pipeline.

4.2.3 Attention block and visualization

In Table 6, we present quantitative comparison of the number of parameters and GFLOPs of attention layer(s). Our attention layer is much lighter than that of GCA-Matting in both parameter number and GFLOPs aspects, which shows the effectiveness of our attention. In Fig. 1, we visualize the global attention weight map of given image query patch denoted by red box and the reconstructed alpha feature A' . The brighter the color is, the larger attention weight (pixel value) the pixel holds. The weights of known and unknown part are shown in the top-left corner of each attention map. It is obvious that our attention module can not only select color-relevant pixels accurately but also capture long-distance pixel-to-pixel relationships. The reorganized alpha feature shown on the right of each row demonstrates that the encoder has already concentrated on unknown areas exquisitely which can promote better feature reconstruction in the decoder.

4.2.4 Ablation study on coarse segmentation input

In this section, we present ablation study about coarse foreground segmentation input on Net-T and JI.

Net-T: We conduct an ablation study to investigate the effect of quality of coarse segmentation on Net-T. We test Net-T with *initial segmentation* eroded by 20, 30, 40, and 50 pixels, which simulates flawed applied circumstances, on Composition-1k and Distinctions-646 testsets as shown in Table 5 (a). The accuracy is all above 90% and the mean IoU of unknown region is fluctuating around 0.80, which implies that Net-T is anti-jamming for unperfect foreground segmentation and capable of offering correct trimap estimation.

⁴CAM with ME+CE+lap

JJ: To research how segmentation affects trimap-free JI pipeline, we test JIS and JIH with *initial segmentation* eroded by 20, 30, 40, and 50 pixels on Composition-1k and Distinctions-646 testset. The results are illustrated in Table 5 (b). The deviation of each metric is quite slight and most metrics in their worst performance still set a state-of-the-art record, which reveals that our network can still attain robust property when soft segmentation is in an ill-posed state.⁵

5. Conclusion

In this paper, we propose a novel two-stage trimap-free image matting network, which can predict accurate alpha matte from RGB image and its coarse foreground segmentation. Our matting pipeline can be easily integrated with other state-of-the-art semantic segmentation/salient object detection/matting methods to boost trimap-free matting in real world. Benefiting from semantic information provided by coarse foreground segmentation, our approach employs Trimap Generation Network to capture target objects roughly. The light-weight Non-local Matting Network with Refinement dedicates to transition region under predicted-trimap guidance. Comprehensive experiments indicate that our approach reaches state-of-the-art performance on the Composition-1k test dataset, alphamattng.com benchmark, Distinctions-646 testset, and real imagery in trimap-needed and trimap-free cases.

Acknowledgments

This paper was supported by funding 2019-INT007 from the Shenzhen Institute of Artificial Intelligence and Robotics for Society. Thank Zhixiang Wang, Junjie Hu and Kangfu Mei for comments.

References

- [1] Yağiz Aksoy, Tae-Hyun Oh, Sylvain Paris, Marc Pollefeys, and Wojciech Matusik. Semantic soft segmentation. *ACM Transactions on Graphics (TOG)*, 37(4):1–13, 2018. [2](#)
- [2] Yağiz Aksoy, Tunc Ozan Aydin, and Marc Pollefeys. Designing effective inter-pixel information flow for natural image matting. In *Proceedings of the IEEE Conference on Computer Vision and Pattern Recognition*, pages 29–37, 2017. [2](#)
- [3] Ahmad Al-Kabbany and Eric Dubois. A novel framework for automatic trimap generation using the gestalt laws of grouping. In *Visual Information Processing and Communication VI*, volume 9410, page 94100G. International Society for Optics and Photonics, 2015. [3](#)
- [4] Md Amirul Islam, Mahmoud Kalash, and Neil DB Bruce. Revisiting salient object detection: Simultaneous detection, ranking, and subitizing of multiple salient objects. In *Proceedings of the IEEE Conference on Computer Vision and Pattern Recognition*, pages 7142–7150, 2018. [4](#)
- [5] Jimmy Ba, Volodymyr Mnih, and Koray Kavukcuoglu. Multiple object recognition with visual attention. *arXiv preprint arXiv:1412.7755*, 2014. [3](#)
- [6] Dzmitry Bahdanau, Kyunghyun Cho, and Yoshua Bengio. Neural machine translation by jointly learning to align and translate. *arXiv preprint arXiv:1409.0473*, 2014. [3](#)
- [7] Denny Britz, Anna Goldie, Minh-Thang Luong, and Quoc Le. Massive exploration of neural machine translation architectures. *arXiv preprint arXiv:1703.03906*, 2017. [3](#)
- [8] Shaofan Cai, Xiaoshuai Zhang, Haoqiang Fan, Haibin Huang, Jiangyu Liu, Jiaming Liu, Jiaying Liu, Jue Wang, and Jian Sun. Disentangled image matting. In *Proceedings of the IEEE International Conference on Computer Vision*, pages 8819–8828, 2019. [2](#), [7](#), [13](#), [14](#)
- [9] Liang-Chieh Chen, George Papandreou, Florian Schroff, and Hartwig Adam. Rethinking atrous convolution for semantic image segmentation. *arXiv preprint arXiv:1706.05587*, 2017. [3](#)
- [10] Quan Chen, Tiezheng Ge, Yanyu Xu, Zhiqiang Zhang, Xinxin Yang, and Kun Gai. Semantic human matting. In *Proceedings of the 26th ACM international conference on Multimedia*, pages 618–626, 2018. [2](#), [3](#), [5](#), [6](#)
- [11] Qifeng Chen, Dingzeyu Li, and Chi-Keung Tang. Knn matting. *IEEE transactions on pattern analysis and machine intelligence*, 35(9):2175–2188, 2013. [2](#)
- [12] Zhenpeng Chen, Yuanjie Zheng, Xiaojie Li, Rong Luo, Weikuan Jia, Jian Lian, and Chengjiang Li. Interactive trimap generation for digital matting based on single-sample learning. *Electronics*, 9(4):659, 2020. [3](#)
- [13] Donghyeon Cho, Sunyeong Kim, Yu-Wing Tai, and In So Kweon. Automatic trimap generation and consistent matting for light-field images. *IEEE transactions on pattern analysis and machine intelligence*, 39(8):1504–1517, 2016. [3](#)
- [14] Donghyeon Cho, Yu-Wing Tai, and Inso Kweon. Natural image matting using deep convolutional neural networks. In *European Conference on Computer Vision*, pages 626–643. Springer, 2016. [1](#), [2](#)
- [15] Yung-Yu Chuang, Brian Curless, David H Salesin, and Richard Szeliski. A bayesian approach to digital matting. In *Proceedings of the 2001 IEEE Computer Society Conference on Computer Vision and Pattern Recognition. CVPR 2001*, volume 2, pages II–II. IEEE, 2001. [2](#)
- [16] Zijun Deng, Xiaowei Hu, Lei Zhu, Xuemiao Xu, Jing Qin, Guoqiang Han, and Pheng-Ann Heng. R3net: Recurrent residual refinement network for saliency detection. In *Proceedings of the 27th International Joint Conference on Artificial Intelligence*, pages 684–690. AAAI Press, 2018. [3](#), [4](#)
- [17] Jun Fu, Jing Liu, Haijie Tian, Yong Li, Yongjun Bao, Zhiwei Fang, and Hanqing Lu. Dual attention network for scene segmentation. In *Proceedings of the IEEE Conference on Computer Vision and Pattern Recognition*, pages 3146–3154, 2019. [3](#)

⁵Please refer to supplementary materials for more detailed ablation study and visual samples.

- [18] Eduardo SL Gastal and Manuel M Oliveira. Shared sampling for real-time alpha matting. In *Computer Graphics Forum*, volume 29, pages 575–584. Wiley Online Library, 2010. 2
- [19] Leo Grady, Thomas Schiwietz, Shmuel Aharon, and Rüdiger Westermann. Random walks for interactive alpha-matting. In *Proceedings of VIIP*, volume 2005, pages 423–429, 2005. 2
- [20] Karol Gregor, Ivo Danihelka, Alex Graves, Danilo Jimenez Rezende, and Daan Wierstra. Draw: A recurrent neural network for image generation. *arXiv preprint arXiv:1502.04623*, 2015. 3
- [21] Vikas Gupta and Shanmuganathan Raman. Automatic trimap generation for image matting. In *2016 International Conference on Signal and Information Processing (ICONSIP)*, pages 1–5. IEEE, 2016. 3
- [22] Kaiming He, Christoph Rhemann, Carsten Rother, Xiaoou Tang, and Jian Sun. A global sampling method for alpha matting. In *CVPR 2011*, pages 2049–2056. IEEE, 2011. 2
- [23] Qiqi Hou and Feng Liu. Context-aware image matting for simultaneous foreground and alpha estimation. In *Proceedings of the IEEE International Conference on Computer Vision*, pages 4130–4139, 2019. 5, 7, 8, 13, 14
- [24] Chang-Lin Hsieh and Ming-Sui Lee. Automatic trimap generation for digital image matting. In *2013 Asia-Pacific Signal and Information Processing Association Annual Summit and Conference*, pages 1–5. IEEE, 2013. 3
- [25] Zilong Huang, Xinggang Wang, Lichao Huang, Chang Huang, Yunchao Wei, and Wenyu Liu. Ccnet: Criss-cross attention for semantic segmentation. In *Proceedings of the IEEE International Conference on Computer Vision*, pages 603–612, 2019. 3
- [26] Saumya Jetley, Nicholas A Lord, Namhoon Lee, and Philip HS Torr. Learn to pay attention. *arXiv preprint arXiv:1804.02391*, 2018. 3
- [27] Zhanghan Ke, Kaican Li, Yurou Zhou, Qiuhua Wu, Xiangyu Mao, Qiong Yan, and Rynson WH Lau. Is a green screen really necessary for real-time human matting? *arXiv preprint arXiv:2011.11961*, 2020. 2
- [28] Philip Lee and Ying Wu. Nonlocal matting. In *CVPR 2011*, pages 2193–2200. IEEE, 2011. 2
- [29] Anat Levin, Dani Lischinski, and Yair Weiss. A closed-form solution to natural image matting. *IEEE transactions on pattern analysis and machine intelligence*, 30(2):228–242, 2007. 2
- [30] Anat Levin, Alex Rav-Acha, and Dani Lischinski. Spectral matting. *IEEE transactions on pattern analysis and machine intelligence*, 30(10):1699–1712, 2008. 2
- [31] Jizhizi Li, Jing Zhang, Stephen J Maybank, and Dacheng Tao. End-to-end animal image matting. *arXiv preprint arXiv:2010.16188*, 2020. 2
- [32] Yaoyi Li and Hongtao Lu. Natural image matting via guided contextual attention. In *Proceedings of the AAAI Conference on Artificial Intelligence*, volume 34, pages 11450–11457, 2020. 1, 2, 3, 4, 5, 7, 8, 13, 14
- [33] Guosheng Lin, Anton Milan, Chunhua Shen, and Ian Reid. Refinenet: Multi-path refinement networks for high-resolution semantic segmentation. In *Proceedings of the IEEE conference on computer vision and pattern recognition*, pages 1925–1934, 2017. 4
- [34] Shanchuan Lin, Andrey Ryabtsev, Soumyadip Sengupta, Brian Curless, Steve Seitz, and Ira Kemelmacher-Shlizerman. Real-time high-resolution background matting. *arXiv preprint arXiv:2012.07810*, 2020. 1, 2
- [35] Hongyu Liu, Bin Jiang, Yi Xiao, and Chao Yang. Coherent semantic attention for image inpainting. In *Proceedings of the IEEE International Conference on Computer Vision*, pages 4170–4179, 2019. 4
- [36] Jinlin Liu, Yuan Yao, Wendi Hou, Miaomiao Cui, Xuansong Xie, Changshui Zhang, and Xian-sheng Hua. Boosting semantic human matting with coarse annotations. In *Proceedings of the IEEE/CVF Conference on Computer Vision and Pattern Recognition*, pages 8563–8572, 2020. 2
- [37] Hao Lu, Yutong Dai, Chunhua Shen, and Songcen Xu. Indices matter: Learning to index for deep image matting. In *Proceedings of the IEEE International Conference on Computer Vision*, pages 3266–3275, 2019. 1, 2, 5, 7, 13, 14
- [38] Minh-Thang Luong, Hieu Pham, and Christopher D Manning. Effective approaches to attention-based neural machine translation. *arXiv preprint arXiv:1508.04025*, 2015. 3
- [39] Sebastian Lutz, Konstantinos Amplianitis, and Aljosa Smolic. Alphagan: Generative adversarial networks for natural image matting. *arXiv preprint arXiv:1807.10088*, 2018. 1, 2, 7
- [40] Xudong Mao, Qing Li, Haoran Xie, Raymond YK Lau, Zhen Wang, and Stephen Paul Smolley. Least squares generative adversarial networks. In *Proceedings of the IEEE international conference on computer vision*, pages 2794–2802, 2017. 12
- [41] Volodymyr Mnih, Nicolas Heess, Alex Graves, et al. Recurrent models of visual attention. *Advances in neural information processing systems*, 27:2204–2212, 2014. 3
- [42] Niki Parmar, Ashish Vaswani, Jakob Uszkoreit, Łukasz Kaiser, Noam Shazeer, Alexander Ku, and Dustin Tran. Image transformer. *arXiv preprint arXiv:1802.05751*, 2018. 3
- [43] R. J. Qian and M. I. Sezan. Video background replacement without a blue screen. In *Proceedings 1999 International Conference on Image Processing (Cat. 99CH36348)*, volume 4, pages 143–146 vol.4, 1999. 1, 2
- [44] Yu Qiao, Yuhao Liu, Xin Yang, Dongsheng Zhou, Mingliang Xu, Qiang Zhang, and Xiaopeng Wei. Attention-guided hierarchical structure aggregation for image matting. In *Proceedings of the IEEE/CVF Conference on Computer Vision and Pattern Recognition*, pages 13676–13685, 2020. 1, 2, 3, 7, 8
- [45] Christoph Rhemann, Carsten Rother, Jue Wang, Margrit Gelautz, Pushmeet Kohli, and Pamela Rott. A perceptually motivated online benchmark for image matting. In *2009 IEEE Conference on Computer Vision and Pattern Recognition*, pages 1826–1833. IEEE, 2009. 7
- [46] Olaf Ronneberger, Philipp Fischer, and Thomas Brox. U-net: Convolutional networks for biomedical image segmentation. In *International Conference on Medical image computing and computer-assisted intervention*, pages 234–241. Springer, 2015. 4

- [47] Soumyadip Sengupta, Vivek Jayaram, Brian Curless, Steven M Seitz, and Ira Kemelmacher-Shlizerman. Background matting: The world is your green screen. In *Proceedings of the IEEE/CVF Conference on Computer Vision and Pattern Recognition*, pages 2291–2300, 2020. 1, 2, 3, 5, 7, 8, 12
- [48] Ehsan Shahrian, Deepu Rajan, Brian Price, and Scott Cohen. Improving image matting using comprehensive sampling sets. In *Proceedings of the IEEE Conference on Computer Vision and Pattern Recognition*, pages 636–643, 2013. 2
- [49] Xiaoyong Shen, Xin Tao, Hongyun Gao, Chao Zhou, and Ji-aya Jia. Deep automatic portrait matting. In *European conference on computer vision*, pages 92–107. Springer, 2016. 2, 3
- [50] Abhinav Shrivastava, Abhinav Gupta, and Ross Girshick. Training region-based object detectors with online hard example mining. In *Proceedings of the IEEE conference on computer vision and pattern recognition*, pages 761–769, 2016. 4
- [51] Sweta Singh, Anand Singh Jalal, and Charul Bhatnagar. Automatic trimap and alpha-matte generation for digital image matting. In *2013 Sixth International Conference on Contemporary Computing (IC3)*, pages 202–208. IEEE, 2013. 3
- [52] Jian Sun, Jiaya Jia, Chi-Keung Tang, and Heung-Yeung Shum. Poisson matting. In *ACM SIGGRAPH 2004 Papers*, pages 315–321. 2004. 2
- [53] Gongbo Tang, Mathias Müller, Annette Rios, and Rico Sennrich. Why self-attention? a targeted evaluation of neural machine translation architectures. *arXiv preprint arXiv:1808.08946*, 2018. 3
- [54] Jingwei Tang, Yagiz Aksoy, Cengiz Oztireli, Markus Gross, and Tunc Ozan Aydin. Learning-based sampling for natural image matting. In *Proceedings of the IEEE Conference on Computer Vision and Pattern Recognition*, pages 3055–3063, 2019. 1, 2, 7, 13, 14
- [55] Ashish Vaswani, Noam Shazeer, Niki Parmar, Jakob Uszkoreit, Llion Jones, Aidan N Gomez, Łukasz Kaiser, and Illia Polosukhin. Attention is all you need. In *Advances in neural information processing systems*, pages 5998–6008, 2017. 3, 4
- [56] Jue Wang and Michael F Cohen. An iterative optimization approach for unified image segmentation and matting. In *Tenth IEEE International Conference on Computer Vision (ICCV’05) Volume 1*, volume 2, pages 936–943. IEEE, 2005. 2
- [57] Jue Wang and Michael F Cohen. Optimized color sampling for robust matting. In *2007 IEEE Conference on Computer Vision and Pattern Recognition*, pages 1–8. IEEE, 2007. 2
- [58] Oliver Wang, Jonathan Finger, Qingxiong Yang, James Davis, and Ruigang Yang. Automatic natural video matting with depth. In *15th Pacific Conference on Computer Graphics and Applications (PG’07)*, pages 469–472. IEEE, 2007. 3
- [59] Xiaolong Wang, Ross Girshick, Abhinav Gupta, and Kaiming He. Non-local neural networks. In *Proceedings of the IEEE conference on computer vision and pattern recognition*, pages 7794–7803, 2018. 3, 4
- [60] Ning Xu, Brian Price, Scott Cohen, and Thomas Huang. Deep image matting. In *Proceedings of the IEEE Conference on Computer Vision and Pattern Recognition*, pages 2970–2979, 2017. 1, 2, 6, 7, 8
- [61] Rui Xu, Xiaoxiao Li, Bolei Zhou, and Chen Change Loy. Deep flow-guided video inpainting. In *Proceedings of the IEEE Conference on Computer Vision and Pattern Recognition*, pages 3723–3732, 2019. 4
- [62] Lu Yang, Qing Song, Zhihui Wang, and Ming Jiang. Parsing r-cnn for instance-level human analysis. In *Proceedings of the IEEE Conference on Computer Vision and Pattern Recognition*, pages 364–373, 2019. 3, 7, 12
- [63] Haichao Yu, Ning Xu, Zilong Huang, Yuqian Zhou, and Humphrey Shi. High-resolution deep image matting. *arXiv preprint arXiv:2009.06613*, 2020. 2, 3, 7, 13, 14
- [64] Jiahui Yu, Zhe Lin, Jimei Yang, Xiaohui Shen, Xin Lu, and Thomas S Huang. Generative image inpainting with contextual attention. In *Proceedings of the IEEE conference on computer vision and pattern recognition*, pages 5505–5514, 2018. 4
- [65] Han Zhang, Ian Goodfellow, Dimitris Metaxas, and Augustus Odena. Self-attention generative adversarial networks. In *International conference on machine learning*, pages 7354–7363. PMLR, 2019. 3
- [66] Yunke Zhang, Lixue Gong, Lubin Fan, Peiran Ren, Qixing Huang, Hujun Bao, and Weiwei Xu. A late fusion cnn for digital matting. In *Proceedings of the IEEE Conference on Computer Vision and Pattern Recognition*, pages 7469–7478, 2019. 1, 2, 3, 7

Appendices

A.1. Introduction

In this supplementary material, we provide our network details, and additional matting details and results.

A.2. Network Structure Details

The Fig. S3, S4, S5, S6, S7, and S8 show our networks in details.

A.3. Matting

A.3.1 Real Data Adaption

In this section, details about the real data adaption are provided.

The pseudo trimap in the adversarial training is generated by segmentation [62] and then erosion of 15 pixels on the foreground and 50 pixels on the background. The soft segmentation for training is produced by erosion on *initial segmentation* from the pseudo trimap with 20 pixels and followed by a Gaussian Blur. The human-finetuned Net-M means finetuning the AIM-pretrained Net-M on combined human images from AIM and Distinctions-646 datasets by the same setting as Net-M except 0.00004 initial learning rate, 10 batch size, and 100,000 iterations. Both pseudo trimap and human-finetuned Net-M serve as teachers for AIM-pretrained Net-T and Net-M. Soft fusion aggregates these two originally separated networks to an end-to-end trimap-free matting network.

In the joint end-to-end training of JI-Real, we follow almost the same settings as Net-T and Net-M, but the learning rate of Net-T is initialized to 0.0001 and the initial learning rate of 0.00004 for Net-M with 6 batch size, 100,000 iterations, and $L_{coarse.\alpha} + L_{refined.\alpha}$ as the regression loss calculated on the whole image and combined with adversarial loss.

27 background videos are collected, either self-captured or from Background Matting [47], to provide background images \bar{B} for image composition in training. We use the similar GAN framework and the same configuration of discriminator as Background Matting [40, 47] to train our generator JI-Real and discriminator D . The overview of real data adaption architecture is shown in Fig. S1. For the generator, we minimize:

$$\min_{\theta_{Real}} E_{X, \bar{B} \sim p_{X, \bar{B}}} [(D(\alpha I + (1 - \alpha)\bar{B}) - 1)^2] + \lambda \{L_{ce} + L_{coarse.\alpha} + L_{refined.\alpha}\}, \quad (6)$$

where $\alpha = \text{JI-Real}(X, \theta_{Real})$, α means the refined alpha matte, X denotes input image I and its coarse segmentation, θ_{Real} is the weights of the JI-Real network, \bar{B} is the given composite background image, λ is 0.5 and reduced by $\frac{1}{2}$ every 10,000 iterations during training, and L_{ce} is the

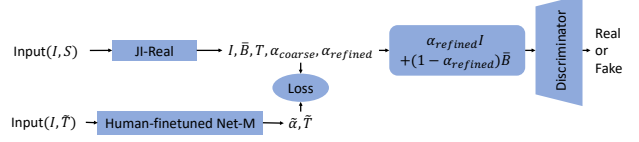


Figure S1: Real Data Adaption Architecture. S is the coarse segmentation of foreground object of image I , \tilde{T} , $\tilde{\alpha}$ are the pseudo trimap and alpha, and T , α_{coarse} , $\alpha_{refined}$ are the predicted trimap, coarse alpha, and refined alpha.

cross-entropy loss of Net-T. For the discriminator, the loss function is

$$\min_{\theta_{Disc}} E_{X, \bar{B} \sim p_{X, \bar{B}}} [(D(\alpha I + (1 - \alpha)\bar{B}))^2] + E_{I \in p_{data}} [(D(I) - 1)^2], \quad (7)$$

where θ_{Disc} is the weights of the discriminator network.

For CAM-1 testing, we use an image and its corresponding previous-mentioned pseudo trimap as input.

A.3.2 Matting Results

Table S1, S2 and S3 show MSE, Gradient and Connectivity Error results of several popular methods including ours on alphamatting.com benchmark, which demonstrates promising performance of our approach. Fig. S2 represents visual comparison of our approach and other methods on alphamatting.com benchmark.

| MSE | Average Rank | | | | Troll | | | Doll | | | Donkey | | | Elephant | | | Plant | | | Pineapple | | | Plastic bag | | | Net | | |
|---|--------------|------------|------|------|-------|-----|-----|------|-----|-----|--------|-----|-----|----------|---|-----|-------|-----|-----|-----------|-----|-----|-------------|-----|-----|-----|-----|-----|
| | Overall | S | L | U | S | L | U | S | L | U | S | L | U | S | L | U | S | L | U | S | L | U | S | L | U | S | L | U |
| Non-local Matting with Refinement(Ours) | 7.5 | 6.1 | 7.1 | 9.4 | 0.2 | 0.2 | 0.3 | 0.1 | 0.2 | 0.2 | 0.1 | 0.1 | 0.1 | 0 | 0 | 0 | 0.4 | 0.5 | 0.8 | 0.1 | 0.1 | 0.3 | 1.1 | 1.3 | 1.1 | 0.7 | 0.8 | 0.9 |
| HDMatt[63] | 7.5 | 10.1 | 6 | 6.5 | 0.3 | 0.3 | 0.4 | 0.2 | 0.2 | 0.3 | 0.1 | 0.1 | 0.1 | 0 | 0 | 0 | 0.4 | 0.4 | 0.6 | 0.1 | 0.2 | 0.2 | 0.9 | 0.9 | 0.9 | 0.8 | 0.8 | 0.8 |
| AdaMatting[8] | 9.9 | 7.6 | 8.9 | 13.1 | 0.3 | 0.4 | 0.4 | 0.2 | 0.2 | 0.3 | 0.2 | 0.2 | 0.2 | 0 | 0 | 0.1 | 0.4 | 0.6 | 1 | 0.1 | 0.2 | 0.3 | 1.1 | 1.2 | 1.1 | 0.6 | 0.6 | 0.6 |
| SampleNet Matting[54] | 10.5 | 7.1 | 10.6 | 13.8 | 0.3 | 0.3 | 0.3 | 0.1 | 0.2 | 0.2 | 0.2 | 0.2 | 0.2 | 0 | 0 | 0.1 | 0.4 | 0.6 | 1.2 | 0.1 | 0.3 | 0.3 | 1.1 | 1.1 | 1.2 | 0.7 | 0.8 | 0.8 |
| GCA Matting[32] | 11.7 | 11.6 | 10.1 | 13.3 | 0.3 | 0.3 | 0.4 | 0.2 | 0.2 | 0.3 | 0.2 | 0.2 | 0.2 | 0 | 0 | 0.1 | 0.5 | 0.6 | 0.8 | 0.2 | 0.2 | 0.5 | 1 | 1.1 | 1.1 | 0.7 | 0.8 | 0.9 |

Table S1: Top-5 MSE results on AlphaMatting benchmark, S, L, U represent the trimap type of small, large and user at the time of submission.

| Gradient | Average Rank | | | | Troll | | | Doll | | | Donkey | | | Elephant | | | Plant | | | Pineapple | | | Plastic bag | | | Net | | |
|---|--------------|------|------|------|-------|-----|-----|------|-----|-----|--------|-----|-----|----------|-----|-----|-------|-----|-----|-----------|-----|-----|-------------|-----|-----|-----|-----|-----|
| | Overall | S | L | U | S | L | U | S | L | U | S | L | U | S | L | U | S | L | U | S | L | U | S | L | U | S | L | U |
| Non-local Matting with Refinement(Ours) | 6.7 | 5.6 | 5.5 | 8.9 | 0.2 | 0.2 | 0.2 | 0.1 | 0.1 | 0.2 | 0.1 | 0.1 | 0.2 | 0.2 | 0.2 | 0.3 | 1 | 1.3 | 2 | 0.5 | 0.5 | 1 | 0.5 | 0.5 | 0.5 | 0.4 | 0.5 | 0.4 |
| HDMatt[63] | 5.6 | 6.5 | 4 | 6.4 | 0.2 | 0.2 | 0.2 | 0.1 | 0.1 | 0.3 | 0.1 | 0.1 | 0.2 | 0.2 | 0.2 | 0.3 | 1.1 | 1.2 | 1.6 | 0.6 | 0.6 | 0.9 | 0.5 | 0.5 | 0.6 | 0.3 | 0.4 | 0.4 |
| AdaMatting[8] | 9.4 | 5.9 | 7 | 15.4 | 0.2 | 0.2 | 0.2 | 0.1 | 0.1 | 0.4 | 0.2 | 0.2 | 0.2 | 0.1 | 0.1 | 0.3 | 1.1 | 1.4 | 2.3 | 0.4 | 0.6 | 0.9 | 0.9 | 1 | 0.9 | 0.3 | 0.4 | 0.4 |
| GCA Matting[32] | 9.7 | 9.9 | 8.1 | 11 | 0.1 | 0.1 | 0.2 | 0.1 | 0.1 | 0.3 | 0.2 | 0.2 | 0.2 | 0.2 | 0.2 | 0.3 | 1.3 | 1.6 | 1.9 | 0.7 | 0.8 | 1.4 | 0.6 | 0.7 | 0.6 | 0.4 | 0.4 | 0.4 |
| Context-aware Matting[23] | 10.9 | 12.4 | 11.6 | 8.6 | 0.2 | 0.2 | 0.2 | 0.1 | 0.2 | 0.2 | 0.2 | 0.2 | 0.2 | 0.2 | 0.4 | 0.4 | 1.4 | 1.5 | 1.8 | 0.8 | 1.3 | 1 | 1.1 | 1.1 | 0.9 | 0.4 | 0.4 | 0.4 |

Table S2: Top-5 Gradient results on AlphaMatting benchmark, S, L, U represent the trimap type of small, large and user at the time of submission.

| Connectivity Error | Average Rank | | | | Troll | | | Doll | | | Donkey | | | Elephant | | | Plant | | | Pineapple | | | Plastic bag | | | Net | | |
|---|--------------|------|-------------|-------------|-------|-----|-----|------|-----|-----|--------|-----|-----|----------|---|---|-------|-----|-----|-----------|-----|-----|-------------|------|-----|-----|-----|-----|
| | Overall | S | L | U | S | L | U | S | L | U | S | L | U | S | L | U | S | L | U | S | L | U | S | L | U | S | L | U |
| Non-local Matting with Refinement(Ours) | 17.3 | 19.7 | 14.7 | 17.4 | 0.9 | 0.9 | 0.9 | 0.1 | 0.1 | 0.1 | 0.2 | 0.2 | 0.2 | 0 | 0 | 0 | 0.1 | 0.1 | 0.2 | 0 | 0 | 0 | 0.9 | 0.7 | 0.9 | 3.2 | 3.3 | 3.2 |
| GCA Matting[32] | 19.7 | 22.9 | 17.3 | 18.9 | 1.1 | 1.1 | 1 | 0.2 | 0.2 | 0.2 | 0.2 | 0.2 | 0.2 | 0 | 0 | 0 | 0.1 | 0.1 | 0.1 | 0 | 0.1 | 0.1 | 1.1 | 1.3 | 1.3 | 1.9 | 1.5 | 1.6 |
| AdaMatting[8] | 21 | 19 | 23.1 | 20.8 | 1.1 | 1.1 | 1.1 | 0.1 | 0.2 | 0.2 | 0.2 | 0.2 | 0.2 | 0 | 0 | 0 | 0.1 | 0.1 | 0.1 | 0 | 0 | 0.1 | 6.8 | 13.3 | 1.4 | 1.3 | 1.3 | 1.3 |
| IndexNet Matting[37] | 23.1 | 21.7 | 24.5 | 23 | 1.3 | 1.3 | 1.3 | 0.1 | 0.1 | 0.1 | 0.2 | 0.2 | 0.2 | 0 | 0 | 0 | 0.1 | 0.1 | 0.3 | 0 | 0.1 | 0.2 | 10 | 10.7 | 1.8 | 1.6 | 1.7 | 1.6 |
| SampleNet Matting[54] | 23.4 | 25 | 21 | 24.5 | 0.9 | 0.9 | 0.8 | 0.1 | 0.1 | 0.1 | 0.2 | 0.2 | 0.2 | 0 | 0 | 0 | 0.1 | 0.1 | 0.2 | 0 | 0.1 | 0.2 | 1.5 | 1.5 | 1.8 | 3.8 | 3.9 | 3.8 |

Table S3: Popular matting approach results of Connectivity Error on AlphaMatting benchmark, S, L, U represent the trimap type of small, large and user at the time of submission.

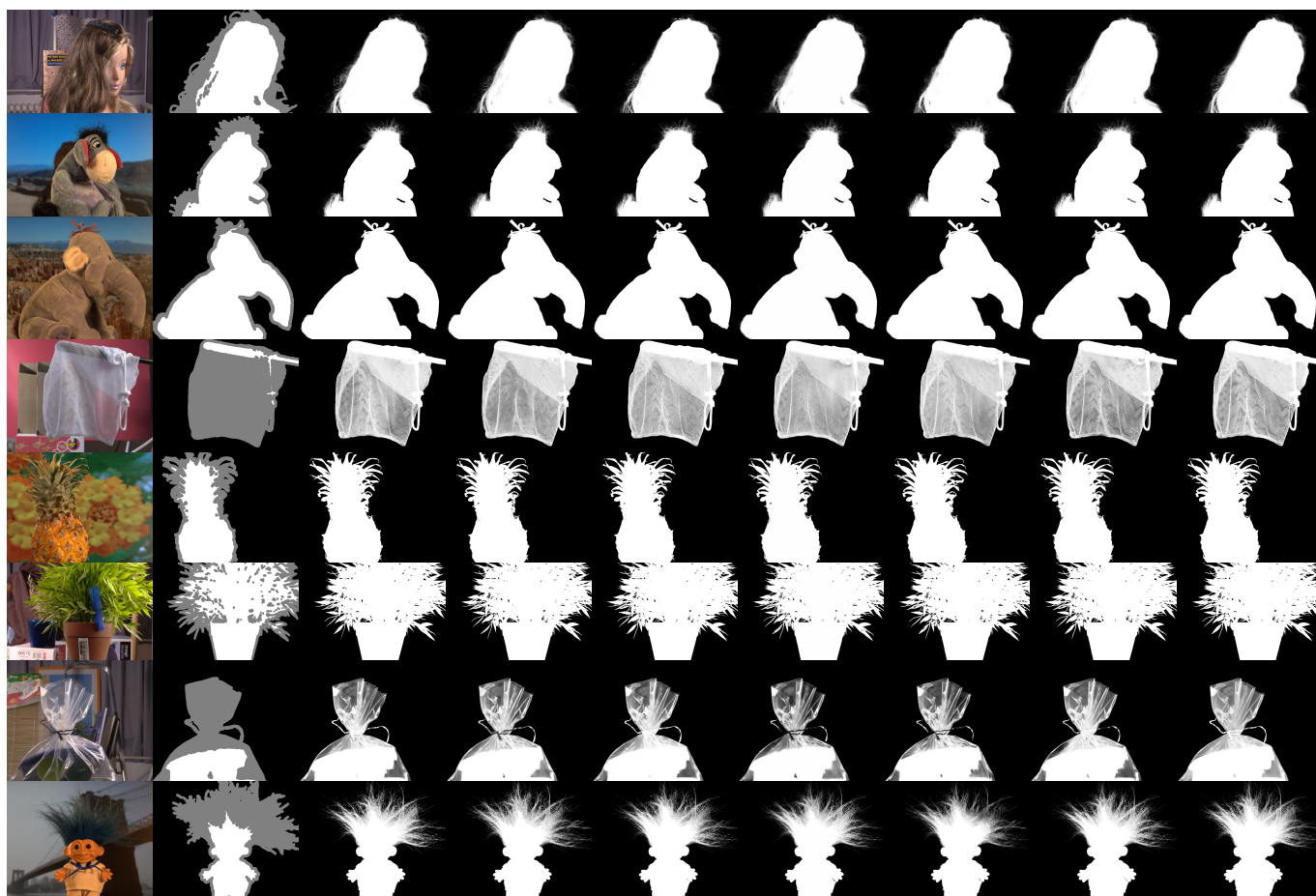


Figure S2: Visual results on alphamattting.com benchmark. From left to right: Image, Trimap (S), HDMatt [63], AdaMatting [8], GCA Matting [32], Context-Aware Matting [23], IndexNet Matting [37], SampleNet Matting [54], and Non-local Matting with Refinement (Ours).

| Block Name | Output Size | Details |
|---|-----------------------------|---|
| Encoder | | |
| Conv+BN+ReLU | $256 \times 256 \times 64$ | 7×7 , 64, stride 2, Bias=False |
| Layer1 | $128 \times 128 \times 256$ | 3×3 max pool, stride=2; Block $\times 3$, stride=[1,1,1], atrous=[1,1,1] |
| Layer2 | $64 \times 64 \times 512$ | Block $\times 4$, stride=[2,1,1,1], atrous=[1,1,1,1] |
| Layer3 | $32 \times 32 \times 1024$ | Block $\times 6$, stride=[2,1,1,1,1,1], atrous=[1,1,1,1,1,1] |
| Layer4 | $32 \times 32 \times 2048$ | Block $\times 3$, stride=[1,1,1], atrous=[1,2,1] |
| Decoder | | |
| ASPP+Dropout | $32 \times 32 \times 256$ | rate of ASPP=1, dropout ratio=0.5; input: output of Layer4 |
| Layer1-Shortcut(Conv2+BN+ReLU) | $128 \times 128 \times 48$ | 1×1 , 48, stride=1, Bias=True; input: output of Layer1 |
| Layer2-Shortcut (Conv3+BN+ReLU) | $128 \times 128 \times 48$ | 1×1 , 48, stride=1, Bias=True; input: 2×2 bilinear upsampling from Layer2 |
| Concatenation Conv (Conv4+BN+ReLU+ Dropout+Conv5+BN+ ReLU+Dropout) | $128 \times 128 \times 48$ | 3×3 , 256, stride=1, Bias=True; 3×3 , 256, stride 1, Bias=True; Dropout ratio2=0.1; input: concatenation of 4×4 bilinear upsampling from ASPP+Dropout, output of Layer2-Shortcut and Layer1-Shortcut |
| Output Conv (Conv6) | $512 \times 512 \times 3$ | 1×1 , 3, stride=1, Bias=True; input: 4×4 bilinear upsampling from Concatenation Conv |

Figure S3: Trimap Generation Network. Block is the Bottleneck of ResNet-atrous from <https://download.pytorch.org/models/resnet50-19c8e357.pth>

| Block Name | Output Size | Details |
|---|----------------------------|---|
| Encoder | | |
| Stride Conv1+SN+BN | $256 \times 256 \times 32$ | $3 \times 3, 32, \text{stride } 2, \text{Bias}=\text{False}$ |
| ShortCut1($2 \times (\text{Conv}+\text{SN}+\text{ReLU}+\text{BN})$) | $512 \times 512 \times 32$ | $3 \times 3, 32, \text{stride}=1, \text{Bias}=\text{False}; \text{input: original image}$ |
| Conv1+SN+BN | $256 \times 256 \times 32$ | $3 \times 3, 32, \text{stride } 1, \text{Bias}=\text{False}$ |
| ShortCut2($2 \times (\text{Conv}+\text{SN}+\text{ReLU}+\text{BN})$) | $256 \times 256 \times 32$ | $3 \times 3, 32, \text{stride}=1, \text{Bias}=\text{False}; \text{input: output of Conv1+SN+BN}$ |
| Stride Conv2+SN+BN | $128 \times 128 \times 64$ | $3 \times 3, 64, \text{stride } 2, \text{Bias}=\text{False}; \text{input: output of Conv1+SN+BN}$ |
| ResBlocks1 | $128 \times 128 \times 64$ | Block $\times 3, \text{stride}=[1,1,1]$ |
| ShortCut3($2 \times (\text{Conv}+\text{SN}+\text{ReLU}+\text{BN})$) | $128 \times 128 \times 64$ | $3 \times 3, 64, \text{stride}=1, \text{Bias}=\text{False}; \text{input: output of ResBlocks1}$ |
| Downsample ResBlock1 | $64 \times 64 \times 128$ | Block $\times 1, \text{stride}=[2]$ |
| ResBlocks2 | $64 \times 64 \times 128$ | Block $\times 3, \text{stride}=[1,1,1]$ |
| Non-local Block | $64 \times 64 \times 128$ | input: image and alpha feature from ResBlocks2 |
| ShortCut4($2 \times (\text{Conv}+\text{SN}+\text{ReLU}+\text{BN})$) | $64 \times 64 \times 128$ | $3 \times 3, 128, \text{stride}=1, \text{Bias}=\text{False}; \text{input: output of Non-local Block}$ |
| Downsample ResBlock2 | $32 \times 32 \times 256$ | Block $\times 1, \text{stride}=[2]$ |
| ResBlocks2 | $32 \times 32 \times 256$ | Block $\times 3, \text{stride}=[1,1,1]$ |
| ShortCut5($2 \times (\text{Conv}+\text{SN}+\text{ReLU}+\text{BN})$) | $32 \times 32 \times 256$ | $3 \times 3, 256, \text{stride}=1, \text{Bias}=\text{False}; \text{input: output of ResBlocks2}$ |
| Downsample ResBlock3 | $16 \times 16 \times 512$ | Block $\times 1, \text{stride}=[2]$ |
| ResBlock3 | $16 \times 16 \times 512$ | Block $\times 1, \text{stride}=[1]$ |
| Decoder | | |
| Upsample ResBlock1 | $32 \times 32 \times 256$ | Block $\times 1, \text{stride}=[2]$ |
| ResBlocks4 | $32 \times 32 \times 256$ | Block $\times 1, \text{stride}=[1]$ |
| Upsample ResBlock2 | $64 \times 64 \times 128$ | Block $\times 1, \text{stride}=[2]; \text{input: the summation of output of ShortCut5 and ResBlocks4}$ |
| ResBlocks5 | $64 \times 64 \times 128$ | Block $\times 2, \text{stride}=[1,1]$ |
| Upsample ResBlock3 | $128 \times 128 \times 64$ | Block $\times 1, \text{stride}=[2]; \text{input: the summation of output of ShortCut4 and ResBlocks5}$ |
| ResBlocks6 | $128 \times 128 \times 64$ | Block $\times 2, \text{stride}=[1,1]$ |
| Upsample ResBlock4 | $256 \times 256 \times 32$ | Block $\times 1, \text{stride}=[2]; \text{input: the summation of output of ShortCut3 and ResBlocks6}$ |
| ResBlocks7 | $256 \times 256 \times 32$ | Block $\times 1, \text{stride}=[1]$ |
| Deconv1+SN+BN | $512 \times 512 \times 32$ | $4 \times 4, 32, \text{stride}=2, \text{bias}=\text{False}; \text{input: the summation of output of ShortCut2 and ResBlocks7}$ |
| Conv2+SN+BN | $512 \times 512 \times 1$ | $3 \times 3, 1, \text{stride}=1, \text{bias}=\text{True}; \text{input: the summation of output of ShortCut1 and Deconv1+SN+BN}$ |

Figure S4: Non-local Matting. ResBlock, ResBlock with downsampling and upsampling are shown in following figures.

| Block Name | Details |
|------------------|--|
| Conv1+SN+BN+ReLU | 3×3 , stride=1, bias=False |
| Conv2+SN+BN | 3×3 , stride=1, bias=False |
| ReLU | input: the summation of original block input and output of Conv2+SN+BN |

Figure S5: ResBlock in Encode. In the decoder, ReLU is replaced with LeakyReLU.

| Block Name | Details |
|--------------------|--|
| Conv1+SN+BN+ReLU | 3×3 , stride=2, bias=False |
| Conv2+SN+BN | 3×3 , stride=1, bias=False |
| Downsampling Layer | 2×2 Avg Pool; input: original block input |
| ReLU | input: the summation of output of Downsampling Layer and Conv2+SN+BN |

Figure S6: ResBlock with Downsampling

| Block Name | Details |
|-------------------------|--|
| DeConv1+SN+BN+LeakyReLU | 4×4 , stride=2, bias=False |
| Conv2+SN+BN | 3×3 , stride=1, bias=False |
| Upsampling Layer | Nearest Upsampling; input: original block input |
| LeakyReLU | input: the summation of output of Upsampling Layer and Conv2+SN+BN |

Figure S7: ResBlock with Upsampling

| Block Name | Output Size | Details |
|------------------------|----------------------------|---|
| Encoder | | |
| Conv0 | $512 \times 512 \times 1$ | $3 \times 3, 1, \text{stride}=1, \text{Bias}=\text{True}$ |
| Conv1+BN+ReLU+MaxPool | $256 \times 256 \times 64$ | $3 \times 3, 64, \text{stride}=1, \text{Bias}=\text{True}; 2 \times 2 \text{ Max Pool}$ |
| Conv2+BN+ReLU+MaxPool | $128 \times 128 \times 64$ | $3 \times 3, 64, \text{stride}=1, \text{Bias}=\text{True}; 2 \times 2 \text{ Max Pool}$ |
| Conv3+BN+ReLU+MaxPool | $64 \times 64 \times 64$ | $3 \times 3, 64, \text{stride}=1, \text{Bias}=\text{True}; 2 \times 2 \text{ Max Pool}$ |
| Conv4+BN+ReLU+MaxPool | $32 \times 32 \times 64$ | $3 \times 3, 64, \text{stride}=1, \text{Bias}=\text{True}; 2 \times 2 \text{ Max Pool}$ |
| Decoder | | |
| Conv5+BN+ReLU+Upsample | $64 \times 64 \times 64$ | $3 \times 3, 64, \text{stride}=1, \text{Bias}=\text{True}; 2 \times 2 \text{ bilinear upsampling};$ input: output of Conv4+BN+ReLU+MaxPool |
| Conv6+BN+ReLU+Upsample | $128 \times 128 \times 64$ | $3 \times 3, 64, \text{stride}=1, \text{Bias}=\text{True}; 2 \times 2 \text{ bilinear upsampling};$ input: concatnation of output of Conv5+BN+ReLU+Upsample and Conv4+BN+ReLU+MaxPool |
| Conv7+BN+ReLU+Upsample | $256 \times 256 \times 64$ | $3 \times 3, 64, \text{stride}=1, \text{Bias}=\text{True}; 2 \times 2 \text{ bilinear upsampling};$ input: concatnation of output of Conv6+BN+ReLU+Upsample and Conv3+BN+ReLU+MaxPool |
| Conv8+BN+ReLU+Upsample | $512 \times 512 \times 64$ | $3 \times 3, 64, \text{stride}=1, \text{Bias}=\text{True}; 2 \times 2 \text{ bilinear upsampling};$ input: concatnation of output of Conv7+BN+ReLU+Upsample and Conv2+BN+ReLU+MaxPool |
| Conv9+BN+ReLU | $512 \times 512 \times 64$ | $3 \times 3, 64, \text{stride}=1, \text{Bias}=\text{True}; 2 \times 2 \text{ bilinear upsampling};$ input: concatnation of output of Conv8+BN+ReLU+Upsample and Conv1+BN+ReLU+MaxPool |
| Conv10 | $512 \times 512 \times 1$ | $3 \times 3, \text{stride}=1, \text{bias}=\text{True};$ input: output of Conv9+BN+ReLU |
| Residual | $512 \times 512 \times 1$ | summation of output of Conv10 and original network input coarse alpha |

Figure S8: Refinement Module